

Host-pathogen dynamics in fungal diseases: Comparing SI and multi-infection models

Noam Ross^{a,*}

^a*Department of Environmental Science and Policy University of California-Davis 1 Shields Avenue Davis, CA 95616 USA*

Abstract

Emerging fungal disease pose major threats to plants and wildlife. As effects of many fungal diseases are load-dependent, they may be better represented by models with variable loads (multi-infection), rather than susceptible-infected (SI) models. I compare equilibrium and transient behavior between these model types, including the dynamics of age structure. To compare models with different structure, I parameterized multi-infection models to replicate SI behavior at either initial or equilibrium phases of an epidemic, comparing the resultant behavior at other phases. Multi-infection diseases have either slower initial growth rates of disease than SI models, or have greater population-suppressing effects. Multi-infection models also produce greater relative mortality in older host stages, and greater overall changes in population age structure, than SI models. These results indicate that using SI models to predict epidemic behavior when diseases are load-dependent may underestimate long-term effects.

Introduction

Emerging fungal infections pose major threats to plant and animal wildlife populations as well as livestock and crops. Fungal life-history traits, including high virulence, long-lived environmental reservoirs, and host generalism are thought to contribute to the potential of these pathogens to drive local and global extinctions of some species (Fisher *et al.* 2012; Eskew & Todd 2013). Oomycetes, a taxonomically distinct group from fungi that nonetheless many of these traits, pose similar threats.

An important component of fungal host-pathogen dynamics is the role of spore load in driving host infection and mortality. Briggs *et al.* (2010) showed that population-level persistence or extinction

*Corresponding author

Email address: nmross@ucdavis.edu (Noam Ross)

16 of mountain yellow-legged frogs (*R. sierrae*) infected by chytrid fungus (*Batrachochytrium*
17 *dendrobatidis*), could be explained by the dynamics of spore load build-up in these populations.
18 Similarly, mortality of bat populations with White Nose Syndrome (*Geomyces destructans*) is
19 closely related to spore load on bat skin, which builds up through bat-to-bat contact over the
20 course of the hibernation period (Langwig *et al.* 2015). The fungal parasite *Metschnikowia*
21 *bicuspidata* kills its *Daphnia* host when the parasite loads are high enough to interfere with cell
22 metabolism (Hall *et al.* 2009). Many mammals, including humans, which are generally resistant
23 to fungal diseases or asymptotic under normal conditions may nonetheless become infected and
24 exhibit symptoms or mortality under persistent exposure to large fungal spore loads (Casadevall
25 2005).

26 Accumulation of local infections, rather than systemic infections, has long been recognized as an
27 important component of plant disease dynamics (Waggoner & Rich 1981; Dobson & Crawley
28 1994; McRoberts *et al.* 2003), especially in cases of parasitic plants such as mistletoe (Martinez
29 & Effects 1996). Sudden Oak Death, caused by the oomycete *Phyophthora ramorum*, kills tanoak
30 (*Notholithocarpus densiflorus*) faster in the presence of large numbers of other infected hosts,
31 indicating that continued accumulation of infections, rather than just disease progress, drives
32 mortality (Cobb *et al.* 2012).

33 Most attempts to model fungal disease dynamics have used traditional susceptible-infected (*SI*)
34 disease frameworks, which represent disease as a binary state of the host (Kermack & Mckendrick
35 1927). Extensions such as susceptible-exposed-infected-removed (*SEIR*) models represent disease
36 progression within hosts, but do not capture the accumulation of *new* infections in hosts that
37 may drive disease impacts. This dynamic may be better captured using the framework created by
38 Anderson & May (1978) to model macroparasite infections, where disease is represented by the
39 number of discrete infections (or parasites), within each host. Here I use the term multi-infection
40 to describe these models.

41 Response to disease outbreak often requires prediction of medium- and long-term behavior from
42 early-phase dynamics of disease, which in turn requires mechanistic disease models. However,
43 in early stages of epidemics of emerging diseases, the importance of disease load may not be
44 known, nor the appropriateness of multi-infection rather than *SI* models. Disease load is often

45 considerably more difficult to measure than prevalence, allowing only observations of susceptible
46 vs. infected states. However, model choice may have considerable influence on predictions of
47 disease dynamics and management response.

48 Age and stage structure is another potentially important factor driving fungal disease dynamics.
49 The effect of Chytrid fungus on frogs varies across life stages (Rachowicz & Vredenburg 2004;
50 Garner *et al.* 2009). Mortality rates in tanoak are much greater in large trees than small ones
51 (Cobb *et al.* 2012). However as organisms can grow over similar time scales as the progress of a
52 fungal epidemic, observed patterns in age-disease relationships can be difficult to disentangle
53 from host-pathogen dynamics.

54 There is a considerable literature on host-pathogen dynamics of in age- and stage-structured
55 populations using *SI* models (Castillo-Chavez *et al.* 1989; Busenberg & Haderler 1990; Diekmann
56 *et al.* 1990; Hethcote 2000; Dietz & Heesterbeek 2002; Klepac & Caswell 2010). There is
57 a somewhat smaller literature on age structure in multi-infecton models. In multi-infection
58 models, Krasnov *et al.* (2006) showed that parasite counts increase with age in rodents. Pacala
59 & Dobson (1988) created a method to detect the mortality effect of macroparasites based of
60 the distribution of parasites among different age groups. Duerr *et al.* (2003) showed how a
61 age-infection relationships could be modified by a variety of age- time- and density-dependent
62 processes, but also showed that interpretation of such age-infection patterns was ambiguous if
63 more than one such process was operating.

64 Here I explore how the transient host-pathogen dynamics differ between *SI* and multi-infection
65 systems. To compare models that with different structures and in which parameters have different
66 interpretations, I fit the models to each other so that they have identical *dynamic behaviors* at
67 different stages of an epidemic. I examine how *SI* and multi-infection models differ in long-term
68 dynamics when parameterized to fit identical short-term conditions, and vice versa. I also explore
69 how patterns of disease across life stages differ between over the course of epidemics in *SI* and
70 multi-infection models.

71 *Methods*

72 *Model Structure*

73 I compared dynamics in 3 ODE-based disease models: A simple *SI* model, a multi-infection
 74 model based on Anderson & May (1978), and an intermediate *SIV* (susceptible-infected-*very*
 75 infected) model.

76 Each model has a two-stage population structure (population N = juveniles J + adults A). New
 77 individuals enter the uninfected, juvenile stage via density-dependent recruitment ($fN(1 - N/K)$,
 78 where f is fecundity and K carrying capacity). Individuals move from juvenile to adult classes
 79 at the transition rate g .

80 Disease transmission is density-dependent; In the *SI* model, susceptible individuals (J_S, A_S)
 81 become infected (J_I, A_I) at a rate equal to the density of infected individuals times the transmis-
 82 sivity of the disease (λ). All individuals die at the a base rate (d), and diseased individuals have
 83 additional mortality (α).

84 The complete *SI* model is

$$\begin{aligned} \frac{dJ_S}{dt} &= fN(1 - N/K) - J_S(d + g + \lambda J_I + \lambda A_I) & \frac{dA_S}{dt} &= gJ_S - A_S(d + \lambda N) \\ \frac{dJ_I}{dt} &= \lambda J_S(J_I + A_I) - J_I(d + g + \alpha) & \frac{dA_I}{dt} &= gJ_I + \lambda A_S(J_I + A_I) - A_I(d + \alpha) \\ N &= J_S + A_S + J_I + A_I \end{aligned}$$

85 Note that this is a *null model* of age structure; neither demographic nor epidemiological parameters
 86 vary with age. When juvenile and adult classes are summed, the growth term g drops out, and
 87 dN/dt is independent of g .

88 The other two models are extensions of the *SI* model with additional disease classes representing
 89 degrees of infection. In the multi-infection model, there are an infinite number of disease classes
 90 designated $i = 0, 1, 2, \dots, \infty$. For purposes of simulation, the number of classes is truncated,
 91 with a maximum value of k . Transmissivity (λ) and mortality (α) are additive in these models,
 92 increasing linearly with i . Trees advance to the next disease class at rate Λ , the overall force of

infection, which is the sum of each tree’s contribution, $i\lambda$. Trees in each stage die at rate $d + i\alpha$.
Here is the complete multi-infection model:

$$\begin{aligned} \frac{dJ_0}{dt} &= fN(1 - N/K) - J_0(d + g + \Lambda) & \frac{dA_0}{dt} &= gJ_0 - A_0(d + \Lambda) \\ \frac{dJ_i}{dt} &= \Lambda dJ_{i-1} - J_i(d + g + i\alpha + \Lambda) & \frac{dA_i}{dt} &= gJ_i + \Lambda A_{i-1} - A_i(d + i\alpha + \Lambda) \\ \frac{dJ_k}{dt} &= \Lambda dJ_{k-1} - J_k(d + g + k\alpha) & \frac{dA_k}{dt} &= gJ_k + \Lambda A_{k-1} - A_k(d + k\alpha) \\ N &= \sum_{i=0}^k J_i + A_i & \Lambda &= \lambda \sum_{i=1}^k i(J_i + A_i) \end{aligned}$$

The *SIV* model is merely a truncated version of the multi-infection model, with $k = 2$. For this model I refer N_0 as S , N_1 as I and N_2 as V , and use S , I , and V , as subscripts for J , and A as well.

In this paper, parameters (e.g., λ and α) are subscripted with param_{SI} , param_{SIV} , or $\text{param}_{\text{multi}}$ when referring to their values in each of the three models. I also use the term “infected” to refer to individuals of either the I class in the *SI* model, or having at least one infection in the *SIV* or multi-infection models.

Multi-infection models typically assume a distribution of infections in order to reduce the infinite system of equations (Anderson & May 1978). Negative-binomial distributions of infections allow tractable analysis of such models and match empirical studies of infection distribution in the wild (Wilson *et al.* 2002). However, reduced models only approximate the full model asymptotically and do not capture transient dynamics (Adler & Kretzschmar 1992), and key assumptions of the reduced model break down in the presence of age structure. Instead, I avoided making such assumptions by simulating the the infinite system of equations truncating at k .

Comparative parameterization

I compared the models’ behaviors under “equivalent” parameterizations. As the models have different structures, parameters in the models have different interpretations. Specifically, λ and α operate on a per-individual basis in the *SI* model, while they operate on a per-infection basis on the *SIV* and multi-infection models.

114 In order to determine equivalent parameterizations between models, I set parameters for the
115 *SI* model to those in Table 1. I then fit the *SIV* and multi-infection models so that they
116 would exhibit identical *behavior* to the *SI* model under different criteria. The behavior of *SIV*
117 and multi-infection models were adjusted by multiplying both the infectivity ($\lambda_{SIV}, \lambda_{multi}$) and
118 disease-induced mortality ($\alpha_{SIV}, \alpha_{multi}$) parameters by a constant c .

119 Initial conditions in simulations were set at the disease-free equilibrium of the system, modified
120 with 1% of both juveniles and adults having a single infection.

Parameter	Symbol	Base Case Value
fecundity	f	1
carrying capacity	K	1
transition rate	g	0.1
mortality	d	0.01
disease-induced mortality	α	0.2
transmissivity	λ	3
max number of infections (<i>SIV</i> /multi-infection)	k	3 / 150

121 Table 1: Base parameters for disease models

122 I examined model behavior in three cases.

- 123 1. **Equilibrium mortality rate.** The first behavioral criterion was identical equilibrium
124 mortality rate across models. c was varied to match the overall disease-induced mortality
125 rate (and thus the total mortality rate) between models. That is, at steady state,

$$\alpha_{SI} = \alpha_{SIV} \frac{I + 2V}{I + V} = \alpha_{multi} \frac{1}{N} \sum_i i N_i$$

- 126 2. **Initial growth and acceleration rates of infected individuals.** Next, c was adjusted
127 such that the first and second derivatives of growth of total infected individuals under
128 initial conditions. That is,

$$\frac{dI}{dt} = \frac{d(I+V)}{dt} = \frac{dN_{i>0}}{dt}, \text{ and}$$

$$\frac{d^2I}{dt^2} = \frac{d^2(I+V)}{dt^2} = \frac{d^2N_{i>0}}{dt^2}$$

at initial conditions of $S \approx N$, $I_{SI} = I_{SIV} = N_{1multi} \approx 0$ and $I_{SIV} = N_{i \geq 2multi} = 0$.

Note that the first condition, of the initial growth rate of infected individuals, is identical at all cases under these initial conditions. Thus, I used only the second derivative to fit parameter values.

3. Time to 10% infection. This criterion was selected to match behavior among models during the early transient period of disease. c was adjusted so that the SIV and multi-infection models would reach 10% infection in the same time period as the SI model. That is,

$$t \Big|_{\frac{I}{S+I}=0.1} = t \Big|_{\frac{I+V}{S+I+V}=0.1} = t \Big|_{\frac{N_{i \geq 1}}{N}=0.1}$$

All simulations were performed in R (R Core Team 2014), using the deSolve package (Soetaert *et al.* 2010) for simulation, the numDeriv package to determine derivatives (Gilbert & Varadhan 2012), and the ggplot2 (Wickham 2009) package for plotting. Code to reproduce these results is archived online (???)

Results

Aggregate dynamics

Models with similar equilibrium behavior differ in initial transient behavior. Figure 1 shows the dynamic behavior of the SI , SIV , and multi-infection models calibrated to equivalent mortality at equilibrium. Under this parameterization, all models reach an internal equilibrium with a population level suppressed from the disease-free equilibrium at which they started. As all other rates are equal, the equilibrium populations are identical between the models, as well.

Under this parameterization, the ratio of α and λ values between the models (c) is the inverse of the mean number of infections at equilibrium in the SIV and multi-infection models. This value is 0.69 for the SIV model and 0.61 for the multi-infection model.

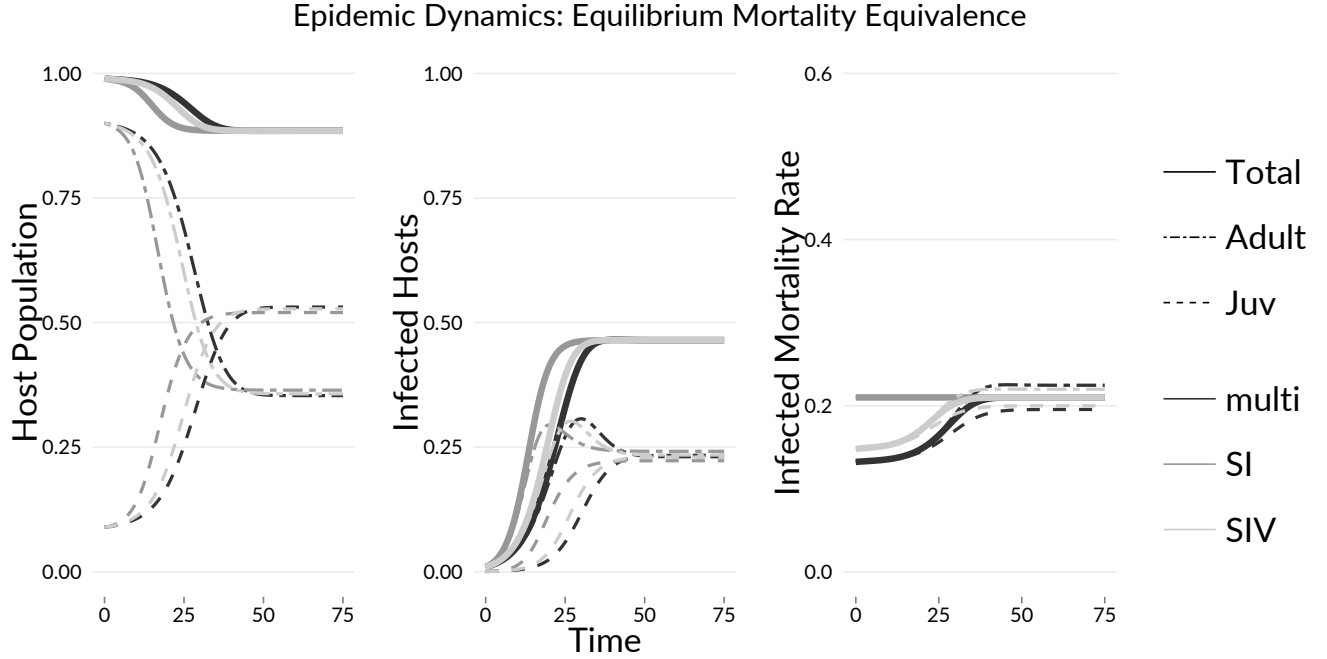


Figure 1: Dynamics of models parameterized to equivalent equilibrium mortality rates

151 In the *SIV* and multi-infection models, the apparent mortality rate of infected individuals
 152 increases over time. Early in the epidemic, individuals have small numbers of infections, thus the
 153 mortality rate across individuals with any level of infection is low. As the epidemic progresses,
 154 the mean number of infections per infected individual increases, raising the mortality rate of the
 155 infected class until equilibrium is reached.

156 The change in mortality rates is driven by changes in the distribution of infections over time,
 157 shown in Figures 2 and 3. As the disease progresses through the population in the *SIV* model,
 158 the proportion of individuals in the *I* and *V* classes increases for both juveniles and adults.
 159 Similarly, in the multi-infection model, the mean number of infections in each individual increases
 160 over time, increasing the mortality rate.

161 While equilibrium behaviors are identical and models start at the same initial conditions, transient
 162 behavior differs. The time to equilibrium is greater in the multi-infection model than the *SIV*
 163 model, and greater in both than the *SI* model. It takes longer in the *SIV* model, and longest in
 164 the multi-infection model, for the disease to emerge.

165 **Models with similar initial behavior reach different equilibrium conditions.** Figure 4
 166 shows the dynamics of the three models in the case where the initial first and second derivatives are

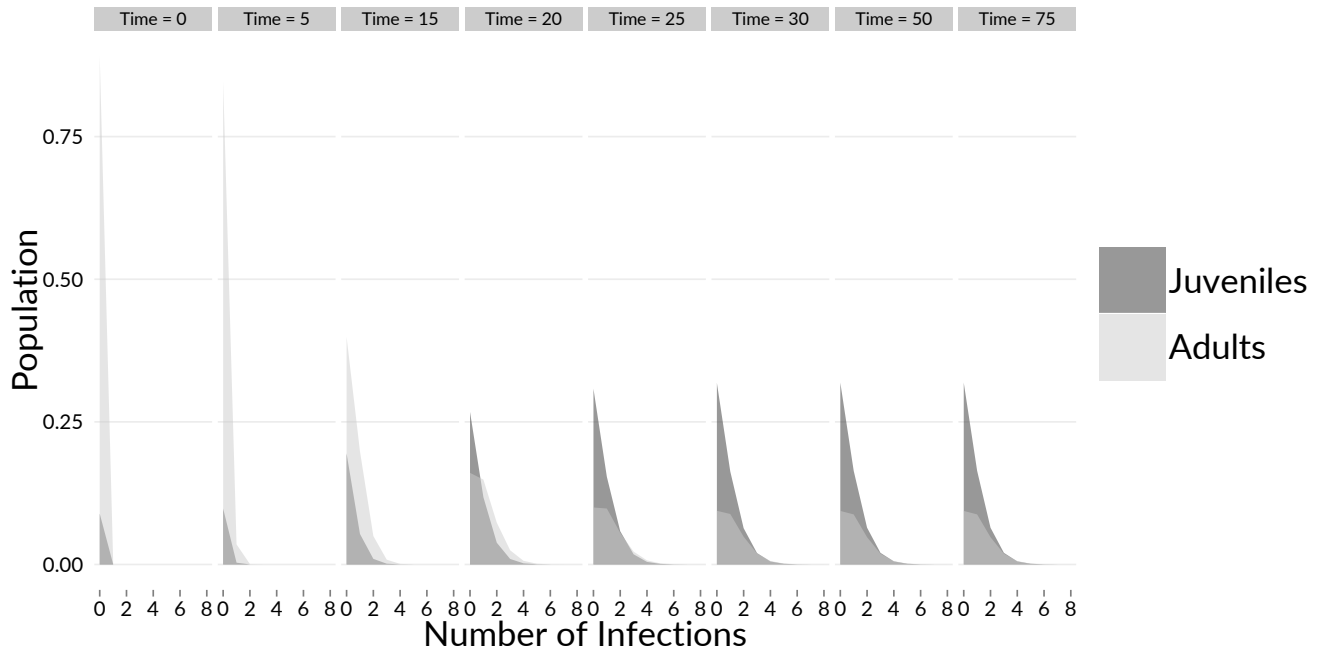


Figure 2: Dynamics infection classes in the SIV model

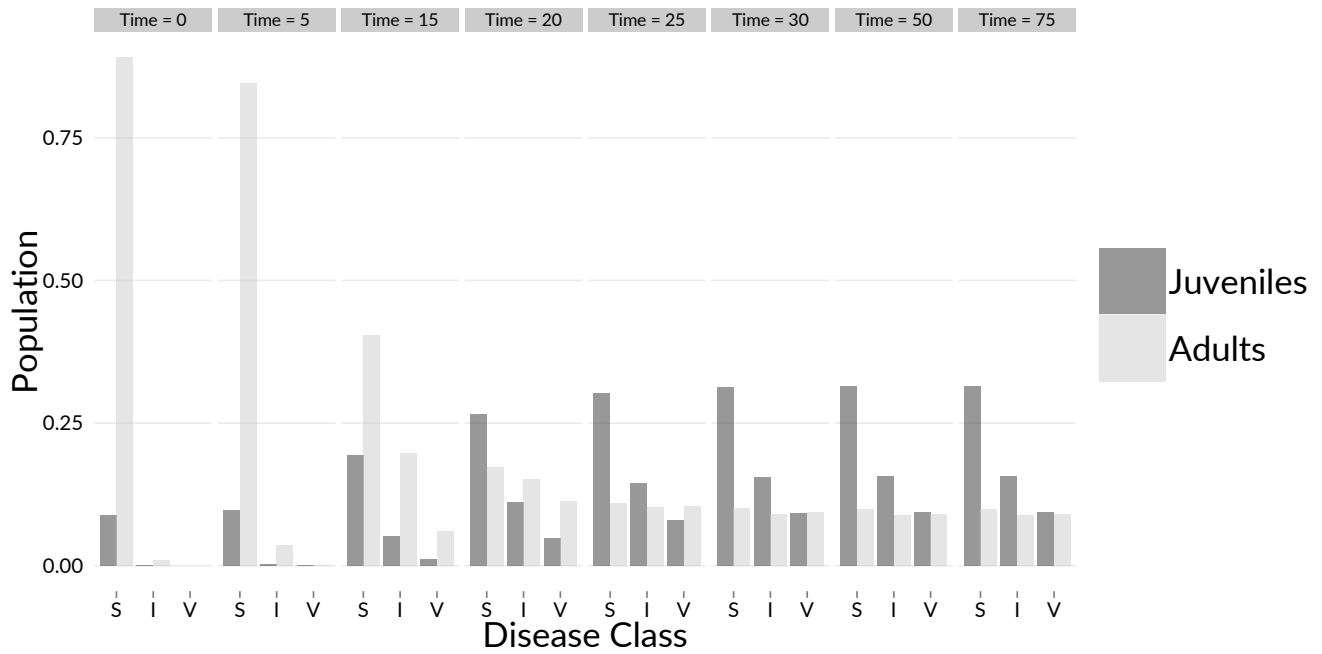


Figure 3: Dynamics of infection classes in the multi-infection model

equivalent. As in the matching-equilibrium parameterizations, mortality for infected individuals increases over time until equilibrium is reached. Unlike that parameterization, per-infection parameters in the *SIV*/multi-infection models (mortality and infectivity), are similar to per-individual parameters in the *SI* model. c is 0.99 for the *SIV* model and 0.99 for the multi-infection model. Total mortality rates for the *SIV* and multi-infection models start at the same levels as the *SI* model and diverge over time.

The *SIV* and multi-infection models have nearly identical behavior. At equilibrium, their populations are suppressed to lower levels than in the *SI* model, and a smaller number of the individuals are infected. This is because the difference in mortality rates of infected individuals between the *SI* and the other models is greater, increasing turnover of infected individuals. In this case, the *SIV* and multi-infection models reach equilibrium *before* the *SI* model.

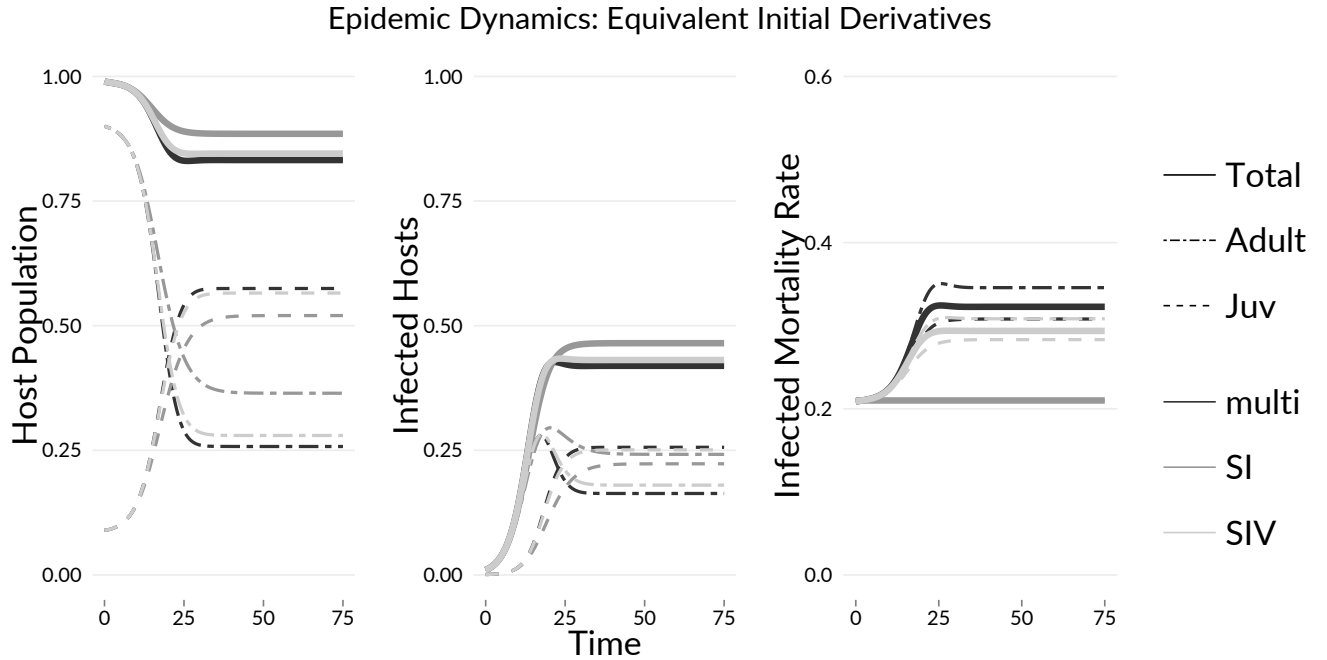


Figure 4: Dynamics of models parameterized to equivalent initial rates of growth of infectious individuals

Figure 5 shows model dynamics when models were parameterized to have equivalent time until 10% of the total population was infected. As with the last parameterization, the initial mortality rates of the *SIV* and multi-infection models are similar to those in the *SI* model; per-infection parameters in *SIV*/multi-infection models are similar to per-individual parameters in the *SI* model. Here c is 0.98 for the *SIV* model and 0.98 for the multi-infection model.

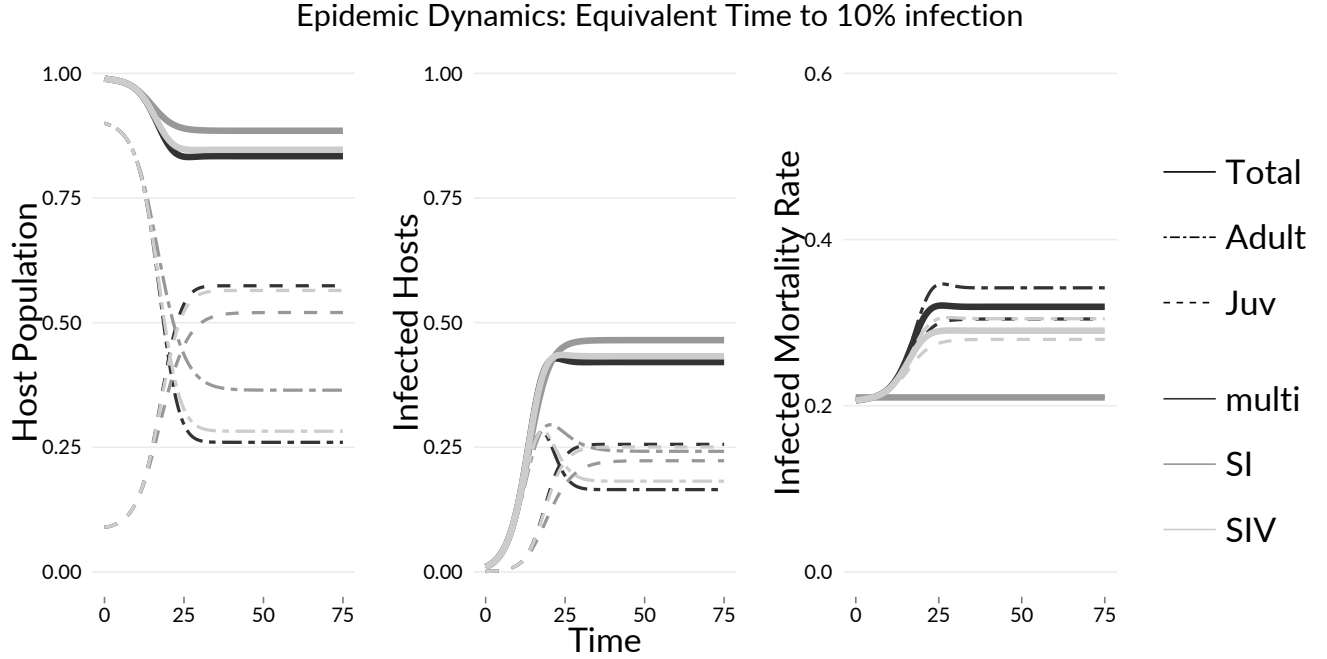


Figure 5: Dynamics of models parameterized to equivalent time to 10% infected individuals

Patterns in the time-to-10%-infection parameterizations are similar to the matched-second-derivative parameterization. Mortality rates for individuals in *SIV* and multi-infection models increase before reaching equilibrium, resulting in lower population sizes and lower populations of infected individuals at equilibrium. Dynamics for the *SIV* and multi-infection models are again very similar, though not as similar as in the matched-derivative case. Also, in this case, the number of infected individuals reaches a peak before going down to reach equilibrium levels.

Age effects

Multi-infection models generate age-dependent effects not found in SI models.

All three models, under all three parameterizations, exhibit some common patterns in the dynamics of population stages. From the disease-free equilibrium dominated by adults, disease outbreak decreases the population of adult stages and increases both the relative and absolute population of the juvenile stages. The infected population of both stages increases, with the adult infected stage reaching a peak before equilibrium and the juvenile infected stage reaching a smaller equilibrium with no peak.

In the equivalent equilibrium mortality parameterization, The *SIV* and multi-infection stage

structures are slower to reach an equilibrium than the *SI* stage structure, with the multi-infection case being slowest. This is similar to the aggregate dynamics for this parameterization. In the case of equivalent initial derivatives, as well as the case of equivalent time to 10% infection, the change in age structure from the disease-free equilibrium is greater in the *SIV* and multi-infection models than the *SI* model. at equilibrium, there are more juveniles and fewer adults in the *SIV*/multi-infection cases.

In the *SIV* and multi-infection models, the mortality rate of infected juveniles and adults increases as the disease progresses, and their mortality rate diverges, with adults having greater mortality rates than juveniles at equilibrium. This occurs in all parameterizations. The reason for this can be found in figures 2 and 3, which show the distribution of infections for both adult and juvenile populations over the course of the epidemic in *SIV* and multi-infection models. Adults and juveniles begin with equal mean numbers of infections, but as the epidemic continues, adult trees accumulate more infections than juveniles by both new infections on adult trees and already-infected juveniles recruiting into the adult population.

In a multi-infection model with age structure, individuals accumulate infections over time, resulting in more infections, and thus greater mortality and infectivity, among older individuals than younger individuals. Even in the absence of age-driven variation in how individuals respond to disease (that is, in a “null model”), different behavior is observed between age groups. In an *SI* model, these differences do not arise.

Discussion

SI and multi-infection models represent disease different ways: as binary states of an individual, or as accumulations of multiple infections across individuals. As a result, they may produce different host-pathogen dynamics. The choice of model structure has important consequences for the prediction of host-pathogen disease dynamics.

Epidemics that appear to be well represented by *SI* models during their outbreak phase may no longer be well represented in later stages if they have dynamics driven by multiple infections. A multi-infection model that behaves like an *SI* model in early stages will diverge from *SI* behavior as increasing infection loads result in greater per-individual mortality rates. I found

226 similar behavior regardless of the criterion used to determine early-phase dynamics (derivatives
227 or time-to-10%-infection). If the multi-infection system system has an equilibrium (other than
228 disease-free or extinction), the host population will be lower at this equilibrium than in an
229 *SI* system due to greater suppression from to disease, while the diseased population itself will
230 be lower as highly infected individuals suppressing population more. A *smaller* fraction of
231 the population will be infected at equilibrium, because of the short survival of highly infected
232 individuals.

233 I found similar patterns in the reverse case, where early disease behavior was predicted from
234 equilibrium behavior using both *SI* and multiple-infection models. Multiple-infection models
235 with the same equilibrium behavior as *SI* models are slower to emerge, as the small numbers of
236 infections on initially infected individuals transmit less disease and kill at slower rates than “fully”
237 infected individuals in the *SI* model, which have higher per-individual transmission mortality.
238 The models converge when mean infection numbers in individuals in the multi-infection model
239 rise such that their virulence matches individuals in the *SI* model.

240 Multiple-infection models indicate that age- or stage-related patterns in disease mortality can
241 arise from the accumulation of infections over time, even in the absence of biological differences
242 among age class in susceptibility to disease. Here I found that, in all parameterizations of
243 multi-infection models, adult mortality rates increased faster than juvenile mortality rates as
244 epidemics progressed, even though per-infection mortality rates were identical between life stages.
245 While in some fungal diseases, host-pathogen interactions drive differences in virulence between
246 life stages (e.g., chytrid fungus, see Rachowicz & Vredenburg (2004)), this difference could explain
247 part or all of stage-related differences in mortality in fungal diseases, such as in Sudden Oak
248 Death (Cobb *et al.* 2012).

249 Multiple infection-models also showed increase population-level age effects of disease. In simula-
250 tions where both *SI* and multi-infection models had similar initial behavior, disease resulted in
251 a shift from adult- to juvenile dominance over the course of the epidemic, but in the multiple-
252 infection model this shift was greater, as adult mortality was greater. Also, adult disease
253 prevalence was lower in the late stages of multiple infection models, because with higher adult
254 mortality diseased adults have short lifespans.

255 Simplified models of multiple infection, such as the *SIV* model presented here, can capture some
 256 of the components of load-driven disease dynamics. Here, the *SIV* model behaved similarly to
 257 the multi-infection model, including similar differences in time-to-equilibrium from the *SI* model,
 258 similar suppression of the final population, similar total infected host number, and age-mortality
 259 patterns. However, there were differences between the *SIV* and multi-infection model in the
 260 apparent mortality rate of infected hosts, especially in the time-to-10%-infection parameterization,
 261 indicating a role of the long tail of hosts with high infection number in driving this pattern.

262 These results indicate that identifying multi-infection driven diseases early in their emergence
 263 will significantly alter predictions of disease dynamics. Can the dynamics of these disease be
 264 distinguished from those of *SI*-like processes in the data from early-stage emerging epidemics,
 265 especially when data are of disease prevalence rather than load? One way to distinguish these
 266 mechanisms is to look for changes in mortality rate as disease progresses or between early-
 267 or late-epidemic populations, or to look for differences in mortality rate among age classes.
 268 Both these patterns can indicate multi-infection-driven processes, though such patterns are not
 269 sufficient to disentangle the multiple processes that may drive mortality patterns. Instead, these
 270 patterns can indicate the potential role of these mechanisms, and the need to investigate the
 271 relationships between infection load and host effects.

272 *References*

- 273 1. Adler, F.R. & Kretzschmar, M. (1992). Aggregation and stability in parasite—host models.
 274 *Parasitology*, 104, 199–205.
- 275 2. Anderson, R. & May, R. (1978). Regulation and stability of host-parasite population interactions:
 276 I. Regulatory processes. *The Journal of Animal Ecology*, 47, 219–247.
- 277 3. Briggs, C.J., Knapp, R. a & Vredenburg, V.T. (2010). Enzootic and epizootic dynamics of the
 278 chytrid fungal pathogen of amphibians. *Proceedings of the National Academy of Sciences of the*
 279 *United States of America*, 107, 9695–700.
- 280 4. Busenberg, S.N. & Haderler, K. (1990). Demography and epidemics. *Mathematical Biosciences*,
 281 101, 63–74.

- 282 5.Casadevall, A. (2005). Fungal virulence, vertebrate endothermy, and dinosaur extinction: is
283 there a connection? *Fungal genetics and biology : FG & B*, 42, 98–106.
- 284 6.Castillo-Chavez, C., Hethcote, H.W., Andreasen, V., Levin, S.A. & Liu, W.M. (1989). Epi-
285 demiological models with age structure, proportionate mixing, and cross-immunity. *Journal of*
286 *Mathematical Biology*, 27, 233–258.
- 287 7.Cobb, R.C., Filipe, J.A.N., Meentemeyer, R.K., Gilligan, C.A. & Rizzo, D.M. (2012). Ecosystem
288 transformation by emerging infectious disease: loss of large tanoak from California forests. *Journal*
289 *of Ecology*, 100, 712–722.
- 290 8.Diekmann, O., Heesterbeek, J. & Metz, J. (1990). On the definition and the computation of
291 the basic reproduction ratio R_0 in models for infectious diseases in heterogeneous populations.
292 *Journal of Mathematical Biology*, 28, 365–382.
- 293 9.Dietz, K. & Heesterbeek, J. (2002). Daniel Bernoulli’s epidemiological model revisited. *Mathe-*
294 *matical Biosciences*, 180, 1–21.
- 295 10.Dobson, A. & Crawley, M. (1994). Pathogens and the structure of plant communities. *Trends*
296 *in Ecology & Evolution*, 9, 393–8.
- 297 11.Duerr, H.P., Dietz, K. & Eichner, M. (2003). On the interpretation of age–intensity profiles
298 and dispersion patterns in parasitological surveys. *Parasitology*, 126, 87–101.
- 299 12.Eskew, E.A. & Todd, B.D. (2013). Parallels in Amphibian and Bat Declines from Pathogenic
300 Fungi. *Emerging Infectious Diseases*, 19, 379–385.
- 301 13.Fisher, M.C., Henk, D. a, Briggs, C.J., Brownstein, J.S., Madoff, L.C. & McCraw, S.L.*et al.*
302 (2012). Emerging fungal threats to animal, plant and ecosystem health. *Nature*, 484, 186–94.
- 303 14.Garner, T.W.J., Walker, S., Bosch, J., Leech, S., Marcus Rowcliffe, J. & Cunningham, A.a.*et*
304 *al.* (2009). Life history tradeoffs influence mortality associated with the amphibian pathogen
305 *Batrachochytrium dendrobatidis*. *Oikos*, 118, 783–791.
- 306 15.Gilbert, P. & Varadhan, R. (2012). *numDeriv: Accurate Numerical Derivatives*.
- 307 16.Hall, S.R., Simonis, J.L., Nisbet, R.M., Tessier, A.J. & Cáceres, C.E. (2009). Resource ecology
308 of virulence in a planktonic host-parasite system: an explanation using dynamic energy budgets.

309 *The American Naturalist*, 174, 149–62.

310 17.Hethcote, H.W. (2000). The Mathematics of Infectious Diseases. *SIAM Review*, 42, 599–653.

311 18.Kermack, W. & Mckendrick, A. (1927). A Contribution to the Mathematical Theory of
312 Epidemics. *Proceedings of the Royal Society of London. Series A: Mathematical and Physical*
313 *Sciences*, 115, 700–721.

314 19.Klepac, P. & Caswell, H. (2010). The stage-structured epidemic: linking disease and demogra-
315 phy with a multi-state matrix approach model. *Theoretical Ecology*, 4, 301–319.

316 20.Krasnov, B.R., Stanko, M. & Morand, S. (2006). Age-dependent flea (Siphonaptera) parasitism
317 in rodents: a host’s life history matters. *The Journal of Parasitology*, 92, 242–8.

318 21.Langwig, K.E., Frick, W.F., Reynolds, R., Parise, K.L., Drees, K.P. & Hoyt, J.R.*et al.* (2015).
319 Host and pathogen ecology drive the seasonal dynamics of a fungal disease, white-nose syndrome.
320 *Proceedings. Biological sciences / The Royal Society*, 282, 10–12.

321 22.Martinez, C. & Effects, C. (1996). Effects of the mistletoe *Tristerix* on the aphyllus reproduc-
322 tion of its cactus host *Echinopsis chilensis*, 3, 437–442.

323 23.McRoberts, N., Hughes, G, L.V. & Madden, L.V. (2003). The theoretical basis and practical
324 application of relationships between different disease intensity measurements in plants. *Annals*
325 *of Applied Biology*, 142, 191–211.

326 24.Pacala, S.W. & Dobson, A.P. (1988). The relation between the number of parasites/host and
327 host age: population dynamic causes and maximum likelihood estimation. *Parasitology*, 96, 197.

328 25.R Core Team. (2014). R: A Language and Environment for Statistical Computing.

329 26.Rachowicz, L.J. & Vredenburg, V.T. (2004). Transmission of *Batrachochytrium dendrobatidis*
330 within and between amphibian life stages. *Diseases of Aquatic Organisms*, 61, 75–83.

331 27.Soetaert, K., Petzoldt, T. & Setzer, R.W. (2010). Solving Differential Equations in R: Package
332 deSolve. *Journal of Statistical Software*, 33, 1–25.

333 28.Waggoner, P.E. & Rich, S. (1981). Lesion distribution, multiple infection, and the logistic
334 increase of plant disease. *Proceedings of the National Academy of Sciences of the United States*
335 *of America*, 78, 3292–5.

- 336 29. Wickham, H. (2009). *Ggplot2*. Springer New York, New York, NY.
- 337 30. Wilson, K., Bjørnstad, O.N., Dobson, A.P., Merler, S., Poglayen, G. & Read, A.F. *et al.* (2002).
- 338 Heterogeneities in macroparasite infections: patterns and processes. In: *The ecology of wildlife*
- 339 *diseases*. pp. 6–44.